Terramechanics-based High-Fidelity Dynamics Simulation for Wheeled Mobile Robot on Deformable Rough Terrain

Liang Ding, Keiji Nagatani, Keisuke Sato, Andres Mora, Kazuya Yoshida, Haibo Gao, Zongquan Deng

***Abstract*—Numerical simulation analysis of the wheeled mobile robots' motion is significant for both their R&D and control phases, especially due to the recent increase in the number of planetary exploration missions. Using the position/orientation of the rover body, and all the joint angles as generalized coordinates, the Jacobian matrices and recursive dynamics model are derived. Terramechanics models for calculating the forces and moments acted on the wheel by the deformable soil are introduced, considering the effect of normal force. A rough terrain modeling method is developed for estimating the wheel-soil interaction area, wheel sinkage and the terminal coordinate. A simulation program including the above techniques is developed with Matlab and SpaceDyn Toolbox. Experimental results of a 4-wheeled mobile robot moving on Toyoura soft sand verifies the fidelity of the simulation. A simulation example of a robot moving on random rough terrain is also presented.**

I. Introduction

The Sojourner and MER rovers have proved the effectiveness of wheeled mobile robots (WMRs) in planetary exploration missions. Future missions will require the robots to traverse over more challenging deformable rough terrain.

Dynamics simulation plays important roles in both the R&D phase and the operation phase of WMRs [1]. During the R&D phase of a WMR, dynamics simulations can be used for mechanical design/evaluation/optimization, mobility performance analysis, control strategy validation, etc. While for the operation phase, dynamics simulation can be used to support 3D predictive display for successive tele-operation (such as a lunar rover) or validate commands sequence for supervision operation (such as a Mars rover).

The dynamics of WMRs is primarily composed of two parts: the multi-rigid-body dynamics of vehicle and wheel-soil interaction terramechanics, which is intricate but important for improving the fidelity of simulation. Some dynamics simulation platforms have been developed based on conventional terrestrial vehicle terramechanics. NASA's Jet Propulsion Laboratory (JPL) developed Rover Analysis, Modeling and Simulation (ROAMS) system for real-time simulation of planetary rovers [2-3], which uses a single degree of freedom Hunt-Crossley compliance system at each wheel to compute the force in the normal direction; and a two degree of freedom compliance system to compute tangent forces with a linear spring-damper model [4]. Based on Bekker's classical terramechanics theory, a computational framework called Locomotion Synthesis (LocSyn) for mobile robots was developed, which combines a simulation for the performance prediction and optimization of configuration parameters [5]. A set of tools has been developed by ESA named RCET (Rover Chassis Evaluation Tools) to support design, selection and optimization of space exploration rovers. It consists of a tractive prediction module (TPM) that deals with the wheel terrain interaction based on traditional Bekker terramechanics theory [6]. The Rover Performance Evaluation Tool (RPET) is a systematic tool for rover chassis evaluation via application of Bekker theory developed by Surrey Space Center and DLR [7]. RCAST, which combines a rigid multi-body dynamics engine available in Matlab with the AS^{2}TM wheel-soil interaction module, was developed to optimize the ExoMars Rover mobility for the evaluation of locomotion subsystem designs [8].

Due to the differences between WMRs and terrestrial vehicles in physical dimension, wheel shape, payload, terrain, running velocity, control mode, etc., it is necessary to examine the applicability of the conventional terramechanics theory and improve it aiming at WMRs. Yoshida et al from SRL (Space Robotics Laboratory), Tohoku university, have been researching on terramechanics for planetary exploration robots [9]. The conventional Wong-Reece terramechanics formula was employed to derive an improved practical model for calculating drawbar pull [10]. In order to analyze the steering performance of a wheel and a rover, the lateral force characteristics of a driving wheel was modeled [11]. Based on the research results of terramechanics models, Ishigami et al built all-wheel dynamics model and analyzed the motion dynamics for wheeled robots [12]. The virtual simulation platform was then used for motion analysis, control strategy verification and path evaluation [13].

This study is an extension of the simulation platform of SRL. A generalized dynamics model for mobile robots considering all the external forces and moments acted on the wheels is deduced in Section II. A high-fidelity moving forward/backward terramechanics model considering wheel lug effect and slip-sinkage [14], as well as a steering model, are introduced in Section III. Section IV describes the method

This work was supported by National High Technology Research and Development Program of China (grant No. 2006AA04Z231), Key Natural Science Foundation of Heilongjiang Province in China (grant No. ZJG0709) and Foundation of Chinese State Key Laboratory of Robotics and System (grant No. SKLRS200801A02), and "111" Project (B07018).

L. Ding, K. Nagatani, K. Sato, A. Mora and K. Yoshida are with Department of Aerospace Engineering, Tohoku University, Aoba 6-6-01, Sendai, 980-8579, Japan (e-mail: {liangding, keiji, keisuke, andresmora, yoshida} @astro.mech.tohoku.ac.jp).

H. Gao, Z. Deng, and L. Ding are with School of Mechatronics Engineering, Harbin Institute of Technology, Harbin 150001, Heilongjiang, China; State Key Laboratory of Robotics and System (HIT), Harbin 150001, Heilongjiang, China (e-mail: gaohaibo@hit.edu.cn, dengzq@hit.edu.cn).

of estimating wheel-soil contact area on deformable soil, calculating wheel sinkage and terminal mechanics transformation matrix. Section V presents the simulation implementation, experimental validation and an example based on deformable rough terrain.

II. Generalized Recursive Dynamics Modeling

A. Recursive Kinematics and Jacobian Matrices

If $\boldsymbol{a}=[a_1 \quad a_2 \quad a_3]^T$, $\boldsymbol{b}=[b_1 \quad b_2 \quad b_3]^T$, define $\tilde{\boldsymbol{a}}=\begin{bmatrix} 0 & -a_3 & a_2 \\ a_3 & 0 & -a_1 \\ -a_2 & a_1 & 0 \end{bmatrix}$, then $\boldsymbol{a}\times\boldsymbol{b}=\tilde{\boldsymbol{a}}\boldsymbol{b}$, $\boldsymbol{b}\times\boldsymbol{a}=-\tilde{\boldsymbol{a}}\boldsymbol{b}=\tilde{\boldsymbol{a}}^T\boldsymbol{b}$.

Let $\boldsymbol{q}=[q_1 \quad q_2 \quad \cdots \quad q_{n_v}]^T$ denote the joint variables, where n_v is the number of joints. The WMRs are articulated multi-body systems with moving base and n_w end-points (wheels). Let $\boldsymbol{q}_s=[q_l \quad q_m \quad q_n \quad \cdots \quad q_s]^T$ denote a branch from the rover body to a wheel, n_s denote the number of elements in $\boldsymbol{q}_s$. Replace the joint number l, m, n, …, s of the branch with 1, 2, 3 …, n_s, as shown in Fig. 1, which also shows the initial coordinate $\{\Sigma_I\}$, coordinates $\{\Sigma_i\}$ attached to link i (i=l, m, n, …, s) and related vectors, where $\boldsymbol{p}_i$ is the position vector of link i, $\boldsymbol{r}_i$, the position vector of the centroid of link i, $\boldsymbol{c}_{ij}$, the link vector from link i to joint j, $\boldsymbol{l}_{ij}$=$\boldsymbol{p}_j$-$\boldsymbol{p}_i$, link vector from joint i to joint j, $\boldsymbol{l}_{ie}$, vector from joint i to end-point e.

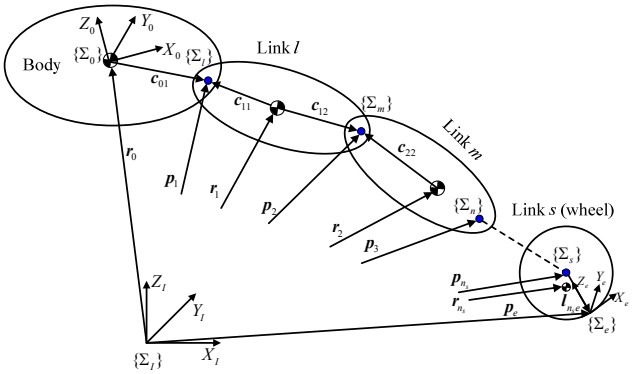

Fig. 1 Coordinates and vectors from rover body to a wheel

The position vector of end-point $\boldsymbol{p}_e$ is:

$$\boldsymbol{p}_e=\boldsymbol{r}_0+\boldsymbol{c}_{01}+\sum_{i=1}^{n_s-1}\boldsymbol{l}_{i(i+1)}+\boldsymbol{l}_{n_s e} \tag{1}$$

The derivative of Eq. (1) is:

$$\begin{aligned}\boldsymbol{v}_e&=\boldsymbol{v}_0+\boldsymbol{\omega}_0\times(\boldsymbol{p}_e-\boldsymbol{r}_0)+\sum_{i=1}^{n_s}\boldsymbol{A}_i\,{}^i\boldsymbol{Z}_i\times(\boldsymbol{p}_e-\boldsymbol{p}_i)\dot{q}_i \\ &=\begin{bmatrix}\boldsymbol{J}_{BTe} & \boldsymbol{J}_{MTe}\end{bmatrix}\begin{bmatrix}\begin{pmatrix}\boldsymbol{v}_0^T & \boldsymbol{\omega}_0^T\end{pmatrix} & \dot{\boldsymbol{q}}^T\end{bmatrix}^T\end{aligned} \tag{2}$$

where $\boldsymbol{J}_{MTe}=[\boldsymbol{L}_{s1}\boldsymbol{A}_1\,{}^1\boldsymbol{Z}_1\times\boldsymbol{P}_{1e} \quad \boldsymbol{L}_{s2}\boldsymbol{A}_2\,{}^2\boldsymbol{Z}_2\times\boldsymbol{P}_{2e} \quad \cdots \quad \boldsymbol{L}_{sn_v}\boldsymbol{A}_{n_v}\,{}^{n_r}\boldsymbol{Z}_{n_v}\times\boldsymbol{P}_{n_v e}]$ is a $3\times n_v$ matrix, and $\boldsymbol{A}_i={}^I\boldsymbol{A}_i$ is the transformation matrix from $\{\Sigma_i\}$ to $\{\Sigma_I\}$[15], ${}^i\boldsymbol{Z}_i=[0 \quad 0 \quad 1]^T$, because the z axis is set to coincide with the joint displacement axis, $\boldsymbol{L}_{ij}$ is an element of matrix $\boldsymbol{L}_{n_v\times n_v}$ to indicate whether the link j is on the access from link 0 to link i ($\boldsymbol{L}_{ij}$=1) or not ($\boldsymbol{L}_{ij}$=0), $\boldsymbol{P}_{ie}$ is the vector from origin of $\{\Sigma_i\}$ to the end point. $\boldsymbol{J}_{BTe}=[\boldsymbol{E} \quad \tilde{\boldsymbol{P}}_{er0}^T]$ is a 3×6 matrix, where $\boldsymbol{P}_{er0}=\boldsymbol{p}_e-\boldsymbol{r}_0$.

The angular velocity of the end-point is:

$$\boldsymbol{\omega}_e=\boldsymbol{\omega}_0+\sum_{i=1}^{n_v}\boldsymbol{A}_i\,{}^i\boldsymbol{Z}_i\dot{q}_i=\begin{bmatrix}\boldsymbol{J}_{BRe} & \boldsymbol{J}_{MRe}\end{bmatrix}\begin{bmatrix}\begin{pmatrix}\boldsymbol{v}_0^T & \boldsymbol{\omega}_0^T\end{pmatrix} & \dot{\boldsymbol{q}}^T\end{bmatrix}^T \tag{3}$$

where $\boldsymbol{J}_{MRe}=[\boldsymbol{L}_{s1}\boldsymbol{A}_1\,{}^1\boldsymbol{Z}_1 \quad \boldsymbol{L}_{s2}\boldsymbol{A}_2\,{}^2\boldsymbol{Z}_2 \quad \cdots \quad \boldsymbol{L}_{sn_v}\boldsymbol{A}_{n_v}\,{}^{n_r}\boldsymbol{Z}_{n_v}]$ is a $3\times n_s$ matrix and $\boldsymbol{J}_{BRe}=[0 \quad \boldsymbol{E}]$ is a 3×6 matrix.

Let $\boldsymbol{J}_e=\begin{bmatrix}\boldsymbol{J}_{Be} & \boldsymbol{J}_{Me}\end{bmatrix}=\begin{bmatrix}\boldsymbol{J}_{BTe} & \boldsymbol{J}_{MTe}\\ \boldsymbol{J}_{BRe} & \boldsymbol{J}_{MRe}\end{bmatrix}$, be the $6\times(6+n_v)$ Jacobian matrix to map the generalized velocity to the end-point; $\dot{\boldsymbol{\Phi}}=\begin{bmatrix}\begin{pmatrix}\boldsymbol{v}_0^T & \boldsymbol{\omega}_0^T\end{pmatrix} & \dot{\boldsymbol{q}}^T\end{bmatrix}^T$, a vector with $(6+n_v)$ elements, i.e., the linear velocity and angular velocity of the body, and the joint velocity. Let $\dot{\boldsymbol{X}}_{ae}$ and $\boldsymbol{J}_{ae}$ denote the velocities of all the wheel-soil interaction points and the corresponding Jacobian matrix:

$$\dot{\boldsymbol{X}}_{ae}=\begin{bmatrix}\boldsymbol{v}_e(1)\\ \boldsymbol{\omega}_e(1)\\ \vdots\\ \boldsymbol{v}_e(n_w)\\ \boldsymbol{\omega}_e(n_w)\end{bmatrix},\quad \boldsymbol{J}_{ae}=\begin{bmatrix}\boldsymbol{J}_e(1)\\ \boldsymbol{J}_e(2)\\ \vdots\\ \boldsymbol{J}_e(n_w)\end{bmatrix},$$

which are $6n_w\times 1$ vector and $6n_w\times(n_v+6)$ matrix, respectively, one obtains:

$$\dot{\boldsymbol{X}}_{ae}=\boldsymbol{J}_{ae}\dot{\boldsymbol{\Phi}} \tag{4}$$

The same method is used to deduce the Jacobian matrix of mapping the velocity from the generalized coordinates to the link centroid, and Eq. (5) is obtained:

$$\dot{\boldsymbol{X}}_a=\boldsymbol{J}_a\dot{\boldsymbol{\Phi}} \tag{5}$$

where $\dot{\boldsymbol{X}}_a$ ($6n_v\times 1$) is the velocity vector of all the centroid, $\boldsymbol{J}_a$ ($6n_v\times(n_v+6)$), the Jacobian matrix. In Eq. (5),

$$\dot{\boldsymbol{X}}_a=\begin{bmatrix}\boldsymbol{v}_1\\ \boldsymbol{\omega}_1\\ \vdots\\ \boldsymbol{v}_{n_v}\\ \boldsymbol{\omega}_{n_v}\end{bmatrix},\quad \boldsymbol{J}_a=\begin{bmatrix}\boldsymbol{J}_1\\ \boldsymbol{J}_2\\ \vdots\\ \boldsymbol{J}_{n_v}\end{bmatrix},\quad \boldsymbol{J}_i=\begin{bmatrix}\boldsymbol{J}_{Bi} & \boldsymbol{J}_{Mi}\end{bmatrix}=\begin{bmatrix}\boldsymbol{J}_{BTi} & \boldsymbol{J}_{MTi}\\ \boldsymbol{J}_{BRi} & \boldsymbol{J}_{MRi}\end{bmatrix},$$

is a $6\times(6+n_v)$ matrix. $\boldsymbol{J}_{BTi}=\begin{bmatrix}\boldsymbol{E} & \tilde{\boldsymbol{r}}_{0i}^T\end{bmatrix}$, $\boldsymbol{J}_{BRi}=\begin{bmatrix}0 & \boldsymbol{E}\end{bmatrix}$, both are 3×6 matrices; $\boldsymbol{J}_{MRi}=\begin{bmatrix}\boldsymbol{L}_{i1}\,{}^1\boldsymbol{Z}_1 & \boldsymbol{L}_{i2}\,{}^2\boldsymbol{Z}_2 & \cdots & \boldsymbol{L}_{in_v}\,{}^{n_v}\boldsymbol{Z}_{n_v}\end{bmatrix}$, $\boldsymbol{J}_{MTi}=\begin{bmatrix}\boldsymbol{L}_{i1}\,{}^1\boldsymbol{Z}_1\times(\boldsymbol{r}_i-\boldsymbol{p}_1) & \boldsymbol{L}_{i2}\,{}^2\boldsymbol{Z}_2\times(\boldsymbol{r}_i-\boldsymbol{p}_2) & \ldots & \boldsymbol{L}_{in_v}\,{}^{n_v}\boldsymbol{Z}_{n_v}\times(\boldsymbol{r}_i-\boldsymbol{p}_{n_v})\end{bmatrix}$, both of which are $3\times n_v$ matrices.

B. Generalized Dynamics Model

Substitute (5) into the kinetic energy equation:

$$T=\frac{1}{2}\sum_{i=0}^{n_v}(\boldsymbol{\omega}_i^T\boldsymbol{I}_i\boldsymbol{\omega}_i+m_i\boldsymbol{v}_i^T\boldsymbol{v}_i)=\frac{1}{2}\dot{\boldsymbol{\Phi}}^T\boldsymbol{H}_{sys}\dot{\boldsymbol{\Phi}} \tag{6}$$

where $\boldsymbol{H}_{sys}$ is the $(n_v+6)\times(n_v+6)$ system generalized inertia matrix [15]:

$$\boldsymbol{H}_{sys}=\begin{bmatrix}M_a(\boldsymbol{E})_{3\times3} & M_a(\tilde{\boldsymbol{r}}_{0g}^T)_{3\times3} & (\boldsymbol{J}_{Tg})_{3\times n_v}\\ M_a(\tilde{\boldsymbol{r}}_{og})_{3\times3} & (\boldsymbol{H}_{\omega})_{3\times3} & (\boldsymbol{H}_{\omega\phi})_{3\times n_v}\\ (\boldsymbol{J}_{Tg}^T)_{n_v\times3} & (\boldsymbol{H}_{\omega\phi}^T)_{n_v\times3} & (\boldsymbol{H}_{\phi})_{n_v\times n_v}\end{bmatrix} \tag{7}$$

where M_a is the overall mass of the robot, $\boldsymbol{r}_{og} = \boldsymbol{r}_g - \boldsymbol{r}_0$,

$\boldsymbol{H}_\omega = \boldsymbol{I}_0 + \sum_{i=1}^{n_v}(\boldsymbol{I}_i + m_i\tilde{\boldsymbol{r}}_{oi}\tilde{\boldsymbol{r}}_{0i}^T) = \boldsymbol{I}_0 + \sum_{i=1}^{n_v}(\boldsymbol{I}_i + m_i\tilde{\boldsymbol{r}}_{0i}^T\tilde{\boldsymbol{r}}_{oi})$,

$\boldsymbol{J}_{Tg} = \sum_{i=0}^{n_v} m_i\boldsymbol{J}_{MTi}$, $\boldsymbol{H}_\phi = \sum_{i=1}^{n_v}(\boldsymbol{J}_{MRi}^T\boldsymbol{I}_i\boldsymbol{J}_{MRi} + m_i\boldsymbol{J}_{MTi}^T\boldsymbol{J}_{MTi})$, and

$\boldsymbol{H}_{\omega\phi} = \sum_{i=1}^{n_v}(\boldsymbol{I}_i\boldsymbol{J}_{MRi} + m_i\tilde{\boldsymbol{r}}_{oi}\boldsymbol{J}_{MTi})$.

According to the Lagrange function:

$$\boldsymbol{F}_{sys} = \boldsymbol{H}_{sys}(\boldsymbol{\Phi})\ddot{\boldsymbol{\Phi}}_{sys} + \boldsymbol{C}(\boldsymbol{\Phi},\dot{\boldsymbol{\Phi}})\dot{\boldsymbol{\Phi}} + \boldsymbol{f}(\dot{\boldsymbol{\Phi}}) + \boldsymbol{G}(\boldsymbol{\Phi}) \tag{8}$$

where $\boldsymbol{C}$ is an $(n_v+6)\times(n_v+6)$ stiffness matrix describing the Coriolis and centripetal effects, which are proportional to $\dot{q}_i^2$ and $\dot{q}_i\dot{q}_j$, respectively, $\boldsymbol{f}$, $(n_v+6)\times 1$ matrix that describes viscous and coulomb friction, negligible for rigid-body dynamics system, $\boldsymbol{G}$, $(n_v+6)\times 1$ gyroscopic vector reflecting the gravity loading, $\boldsymbol{F}_{\text{sys}}$, the vector of generalized forces:

$$\boldsymbol{F}_{sys} = \boldsymbol{N} + \boldsymbol{J}_{ae}{}^T\boldsymbol{N}_{ae} \tag{9}$$

where $\boldsymbol{N}$ is an $(n_v+6)\times 1$ matrix including the forces ($\boldsymbol{F}_0$)/ moments ($\boldsymbol{M}_0$) acted on the body, and those acted on the joints ($\boldsymbol{\tau} = [\tau_1 \quad \tau_2 \quad \cdots \quad \tau_{n_v}]^T$, $\boldsymbol{N}_{ae}$, $6n_w\times 1$ vector including the external forces ($\boldsymbol{F}_e$) and moments ($\boldsymbol{M}_e$) acted on the wheel by soil:

$$\boldsymbol{N} = \begin{bmatrix} \boldsymbol{F}_0 \\ \boldsymbol{M}_0 \\ \boldsymbol{\tau} \end{bmatrix},\ \boldsymbol{N}_{ae} = \begin{bmatrix} \boldsymbol{F}_e(1) \\ \boldsymbol{M}_e(1) \\ \vdots \\ \boldsymbol{F}_e(n_w) \\ \boldsymbol{M}_e(n_w) \end{bmatrix}$$

The dynamics equation of a wheeled mobile robot including wheel-soil interaction terramechanics is:

$$\begin{aligned} &\boldsymbol{H}_{sys}(\boldsymbol{\Phi})\ddot{\boldsymbol{\Phi}}_{sys} + \boldsymbol{C}(\boldsymbol{\Phi},\dot{\boldsymbol{\Phi}})\dot{\boldsymbol{\Phi}} + \boldsymbol{f}(\dot{\boldsymbol{\Phi}}) + \boldsymbol{G}(\boldsymbol{\Phi}) - \\ &\boldsymbol{N} - \boldsymbol{J}_{ae}{}^T\boldsymbol{N}_{ae} = 0 \end{aligned} \tag{10}$$

Let $\boldsymbol{C}(\boldsymbol{\Phi},\dot{\boldsymbol{\Phi}})\dot{\boldsymbol{\Phi}} + \boldsymbol{f}(\dot{\boldsymbol{\Phi}}) + \boldsymbol{G}(\boldsymbol{\Phi}) = \boldsymbol{E}$, the generalized accelerations can be calculated according to Eq. (11):

$$\ddot{\boldsymbol{\Phi}}_{sys} = \boldsymbol{H}_{sys}^{-1}(\boldsymbol{N} + \boldsymbol{J}_{ae}{}^T\boldsymbol{N}_{ae} - \boldsymbol{E}) = 0 \tag{11}$$

Let $\ddot{\boldsymbol{\Phi}}_{sys} = 0$ and $\boldsymbol{N}_{ae} = 0$, there exists $\boldsymbol{N} = \boldsymbol{E}$.

The Newton- Euler equations are:

$$\begin{cases} \boldsymbol{F}_i = m_i\dot{\boldsymbol{v}}_i \\ \boldsymbol{N}_i = \boldsymbol{I}_i\dot{\boldsymbol{\omega}}_i + \boldsymbol{\omega}_i \times \boldsymbol{I}_i\boldsymbol{\omega}_i \end{cases} \tag{12}$$

According to d'Alembert principle, $\boldsymbol{f}_i$ and $\boldsymbol{m}_i$ acted on link i by joint i is:

$$\begin{cases} \boldsymbol{f}_i = \boldsymbol{F}_i - m_i\boldsymbol{g} + \sum_{j=1}^{n}\boldsymbol{S}_{ij}\boldsymbol{f}_j - \boldsymbol{S}_{ei}\boldsymbol{F}_{ei} \\ \boldsymbol{m}_i = \boldsymbol{M}_i + \sum_{j=1}^{n}\boldsymbol{S}_{ij}(\boldsymbol{l}_{ij}\times\boldsymbol{f}_j + \boldsymbol{m}_j) + \boldsymbol{S}_{ii}\times \\ \quad [\lambda_P(i)\boldsymbol{A}_i{}^i\boldsymbol{Z}_i q_i - \boldsymbol{c}_{ii}]\times(\boldsymbol{F}_i - m_i\boldsymbol{g}) - \boldsymbol{S}_{ei}(\boldsymbol{l}_{ie}\times\boldsymbol{F}_{ei} + \boldsymbol{M}_{ei}) \end{cases} \tag{13}$$

where $\lambda_P(i)$ is 1 for a prismatic joint and 0 for rotational joint. The generalized force/moment of link i is:

$$\tau_i = \begin{cases} \boldsymbol{m}_i^T\boldsymbol{A}_i{}^i\boldsymbol{Z}_i & \text{(Rotational joint)} \\ \boldsymbol{f}_i^T\boldsymbol{A}_i{}^i\boldsymbol{Z}_i & \text{(Prismatic joint)} \end{cases} \tag{14}$$

Forces and moments acted on the body are:

$$\begin{cases} \boldsymbol{F}_0 = \sum_{j=0}^{n}\boldsymbol{S}_{0j}\boldsymbol{f}_j + m_0(\dot{\boldsymbol{v}}_0 - \boldsymbol{g}) \\ \boldsymbol{M}_0 = \sum_{j=1}^{n}\boldsymbol{S}_{0j}(\boldsymbol{c}_{0j}\times\boldsymbol{f}_j + \boldsymbol{m}_j) + \boldsymbol{I}_0\dot{\boldsymbol{\omega}}_0 + \boldsymbol{\omega}_0\times\boldsymbol{I}_0\boldsymbol{\omega}_0 \end{cases} \tag{15}$$

where $\boldsymbol{S}$ is the incidence matrix to find the upper connection of a link, $\boldsymbol{S}_{0j}$ is a flag vector to indicate whether j has a connection with the body, $\boldsymbol{S}_{ei}$ is to indicate whether i is an end point.

Let the accelerations of all the generalized coordinates, and the external forces/moments be zero, one can obtain $\boldsymbol{E}$ according to Eqs. (14) and (15).

III. Wheel-soil interaction Terramechanics Models

Each wheel is applied three forces and three moments by the soil, as shown in Fig. 4. The normal force F_N can sustain the wheel. The cohesion and the shearing of the soil can generate a resistance moment M_R and a tractive force; the resistance force is caused by the soil as the wheel sinks into it; the composition of the tractive force and resistance force is called drawbar pull F_{DP}, which is the effective force of driving a wheel. While a wheel is steering or there exists a slip angle, there will be side force F_S, steering resistance moment M_S and overturning moment M_O acted on the wheel.

A. Driving model

Fig. 2 shows the diagram of lugged wheel-soil interaction mechanics [15], where z is the wheel sinkage; θ_1, the entrance angle at which the wheel begins to contact the soil; θ_2, the exit angle at which the wheel looses contact with the soil; θ_m, the angle of maximum stress; θ_1', the angle where the soil starts to deform; W, the vertical load of the wheel; DP, the resistance provided by forward motion, T, the driving torque of the motor; r, the wheel radius; h, the height of lugs; v, the vehicle velocity; and ω, the angular velocity of the wheel. The soil interacts with the wheel in the form of continuous normal stress σ and shearing stress τ, which could be integrated to calculate the interaction mechanics. In order to improve the simulation speed, a simplified closed-form formula [16] is adopted and improved considering the effect of normal force, as given by Eq. (16).

$$\begin{cases} F_N = rbA\sigma_m + r_s bB\tau_m \\ M_R = \dfrac{r_s^2 CD[bc + [1 + c_M(\overline{W} - F_N)/\overline{W}]F_N\tan\varphi/(rA)]}{1 + r_s BD\tan\varphi/(rA)} \\ F_{DP} = [\dfrac{M_R(A^2+B^2)}{r_s AC} - \dfrac{BF_N}{A}](1 + c_{P1} + c_{P2}s)(1 + c_{P3}\dfrac{\overline{W} - F_N}{\overline{W}}) \end{cases} \tag{16}$$

In Eq. (16), c_{P1} and c_{P2} are adopted to reflect the influence of the slip ratio on drawbar pull while θ_m is simplified as a half of θ_1. c_{P3} and c_M are parameters for compensating the effect of normal force, and $\overline{W}$ is the average normal force of the wheels; $\sigma_m = K_s r^N(\cos\theta_m - \cos\theta_1)^N$, $C = (\theta_1 - \theta_2)/2$,

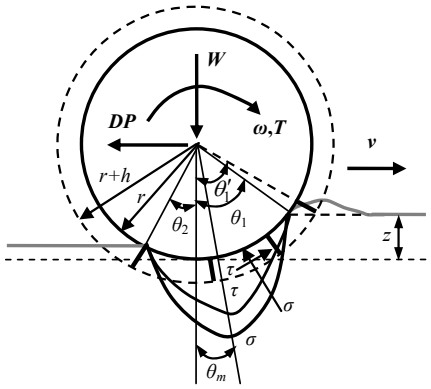

Fig.2 Lugged wheel-soil interaction mechanics diagram

$$A=(\cos\theta_m-\cos\theta_2)/(\theta_m-\theta_2)+(\cos\theta_m-\cos\theta_1)/(\theta_1-\theta_m)\ ,$$

$$B=(\sin\theta_m-\sin\theta_2)/(\theta_m-\theta_2)+(\sin\theta_m-\sin\theta_1)/(\theta_1-\theta_m)\ ,$$

and $\tau_m=(c+\sigma_m\tan\phi)\times(1-\exp\{-r_s[(\theta_1'-\theta_m)-(1-s)(\sin\theta_1'-\sin\theta_m)]/k\})$.

The newly introduced parameters are:

$\theta_1'=\text{acos}[(r-z)/R_j]$, $K_s=k_c/b+k_\varphi$, $N=n_0+n_1 s$, $\theta_2\approx 0$.

The radius R_j is a value between r and r+h for compensating the lug effect [17]. The soil parameters in the equations are: k_c, cohesive modulus, k_φ, frictional modulus, N, an improved soil sinkage exponent, c, cohesion of the soil, φ, the internal friction angle, and k, the shearing deformation modulus, n_0 and n_1 are coefficients for calculating N, which are important in predicting slip-sinkage of wheels.

B. Steering Model

The model for calculating side force F_S is the one introduced in Ref. [11]:

$$F_{S1}=rb\int_{\theta_2}^{\theta_1}\tau_y(\theta)d\theta+\int_{\theta_2}^{\theta_1}R_b(r-h(\theta)\cos\theta)d\theta \quad (17)$$

$$\tau_y(\theta)=[c+\sigma(\theta)]\{1-\exp[-r(1-s)(\theta_1-\theta)\tan\beta/k_y]\} \quad (18)$$

$$R_b=\cot X_c+\tan(X_c+\phi)\left\{hc+\frac{1}{2}\rho h^2\left[(\cot X_c+\frac{\cot X_c^{\,2}}{\cot\phi}\right]\right\} \quad (19)$$

where $X_c=\pi/4-\varphi/2$, k_y is the shearing deformation modulus in y direction, β is the skid angle, h is the height of wheel in the soil.

The overturning moment is approximated with Eq. (20):

$$M_O\approx F_S r \quad (20)$$

The steering resistance moment is considered as zero, and the motion of steering is simulated with kinematics method, as the steering torque has little influence on the motion of the whole rover, and the model is still under development.

IV. Rough Deformable Terrain Geometry Modeling

A. Contact Area Calculation

Literatures usually assume that the wheel soil interaction occurs at a single point for the reason of simplification, which may cause large errors when the robot moves in deformable rough terrain, and even result in failure of simulation because of the abrupt change of wheel sinkage and the forces. Calculating the interaction area of a wheel moving on the soft soil is important for high-fidelity simulation, based on which, the interaction mechanics can be predicted and transformed.

Fig. 3 shows the interaction area of a wheel moving on rough terrain. The known parameters are: (x_w, y_w, z_w), the position of the wheel center W; φ_w, the yaw angle of a wheel, and the Digital Evaluation Map (DEM) of the terrain. The interaction area is simplified as an inclined plane determined by points P_1, P_2 and P_3, the normal vector of which is:

$$\boldsymbol{z_e}=\begin{bmatrix}A_t\\B_t\\C_t\end{bmatrix}=\begin{bmatrix}x_2-x_1\\y_2-y_1\\z_2-z_1\end{bmatrix}\times\begin{bmatrix}x_3-x_1\\y_3-y_1\\z_3-z_1\end{bmatrix} \quad (21)$$

So that the equation of the inclined plane $P_1P_2P_3$ is:

$$A_t(x-x_1)+B_t(y-y_1)+C_t(z-z_1)=0 \quad (22)$$

E, the foot of perpendicular from W to plane $P_1P_2P_3$, is located on line $(x-x_w)/A_t=(y-y_w)/B_t=(z-z_w)/C_t$. The coordinates of point E can be solved by substituting the line equation into Eq. (22). The length of WE is deduced:

$$\overline{WE}=\frac{\left|A_t(x_w-x_1)+B_t(y_w-y_1)+C_t(z_w-z_1)\right|}{\sqrt{A_t^2+B_t^2+C_t^2}} \quad (23)$$

Then, the wheel sinkage is determined by Eq. (24):

$$z=\overline{Ee}=r-\overline{WE} \quad (24)$$

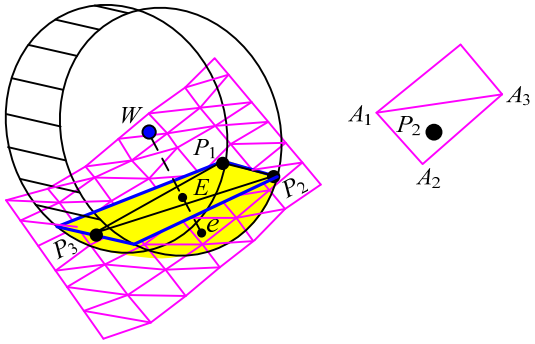

Fig. 3 Interaction area of a wheel moving on deformable rough terrain

Point P_2 is taken as an example to show how to get the coordinates of points P_1, P_2 and P_3. The wheel moving on a random plane can be decomposed into climbing up/down a slope with angle of θ_{cl} and traversing across a slope with inclination angle of θ_{cr}, as shown in Fig. 4. Then, the x and y coordinates of point P_2 is:

$$\begin{cases}x_{P2}=x_w+r\cos\theta_{cr}\\y_{P2}=y_w+r\sin\theta_1\cos\theta_{cl}\end{cases} \quad (25)$$

The coordinates of points A_1, A_2 and A_3 are easy to find by referring to the DEM. z_{P2} can then be determined using the same method as calculating point E.

B. Terminal Force Transformation Matrix

Fig. 4 shows the forces and moments acted on the wheel by the soil. $\{\Sigma_e\}$ and $\{\Sigma_w\}$ are coordinate systems with the same orientation and different origins, at the end point and wheel center, respectively.

$\boldsymbol{x_e}$ is the is the intersection line between wheel-soil interaction plane and the plane with an included angle of φ_w between x axis: $x\tan\varphi_w-y+D'=0$. It is deduced that:

$$\boldsymbol{x_e} = \{C_t, C_t \tan\varphi_w, -A_t - B_t \tan\varphi_w\} \quad (26)$$

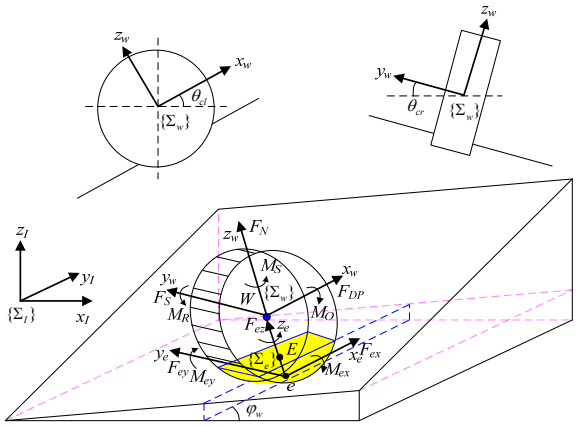

Fig.4 Force analysis of a wheel moving on a random slope

Then, the vector direction of y_e is:

$$\boldsymbol{y_e} = \boldsymbol{z_e} \times \boldsymbol{x_e} = \begin{bmatrix} -A_t B_t - (B_t^2 + C_t^2)\tan\varphi_w \\ C_t^2 + A_t(A_t + B_t \tan\varphi_w) \\ A_t C_t \tan\varphi_w - B_t C_t \end{bmatrix} \quad (27)$$

θ_{cl} (θ_{cr}) is the angle between $\boldsymbol{x}_e$ ($\boldsymbol{y}_e$)and the horizontal plane, which can be calculated by:

$$\begin{cases} \theta_{cl} = \arcsin[(-A_t - B_t \tan\varphi_w)/X_1] \\ \theta_{cr} = \arcsin[C_t(A_t \tan\varphi_w - B_t)/X_2] \end{cases} \quad (28)$$

where $X_1 = \sqrt{C_t^2(1+\tan^2\varphi_w) + (A_t + B_t\tan\varphi_w)^2}$,

$X_2 = \sqrt{X_3[A_t^2 + C_t^2 + 2A_tB_t\tan\varphi_w + (B_t^2 + C_t^2)\tan^2\varphi_w]}$,

$X_3 = \sqrt{A_t^2 + B_t^2 + C_t^2}$. According to $\boldsymbol{x}_e$, $\boldsymbol{y}_e$ and $\boldsymbol{z}_e$, the transformation matrix from $\{\Sigma_e\}$to $\{\Sigma_I\}$ is:

$$\boldsymbol{A}_e = \begin{bmatrix} \frac{C_t}{X_1} & \frac{-A_tB_t - (B_t^2+C_t^2)\tan\varphi_w}{X_2} & \frac{A_t}{X_3} \\ \frac{C_t\tan\varphi_w}{X_1} & \frac{C_t^2 + A_t^2 + A_tB_t\tan\varphi_w}{X_2} & \frac{B_t}{X_3} \\ \frac{-A_t - B_t\tan\varphi_w}{X_1} & \frac{A_tC_t\tan\varphi_w - B_tC_t}{X_2} & \frac{C_t}{X_3} \end{bmatrix} \quad (29)$$

The external forces and torques acted on the wheel-soil interaction point are:

$$\begin{cases} {}^e\boldsymbol{F}_e = {}^w\boldsymbol{F}_e = [F_{DP} \quad F_S \quad F_N]^T \\ {}^e\boldsymbol{M}_e = [M_O - rF_S \quad -M_R + rF_{DP} \quad M_S]^T \end{cases} \quad (30)$$

The equivalent forces and moments acted on the wheel in the initial coordinate $\{\Sigma_I\}$ are:

$$\begin{cases} \boldsymbol{F}_e = \boldsymbol{A}_e\, {}^e\boldsymbol{F}_e \\ \boldsymbol{M}_e = \boldsymbol{A}_e\, {}^e\boldsymbol{M}_e \end{cases} \quad (31)$$

V. Implementation, Validation and Example

A. Simulation Implementation

The numerical simulation program was developed based on Matlab toolbox of SpaceDyn [14]. The principle diagram is shown in Fig. 5. Given DEM terrain, soil parameters, and rover model parameters, the program calculates the wheel-soil interaction area, predicts the external forces acted on the wheel, calculates the accelerations of the generalized coordinates based on the dynamics model, and then integrates them to obtain their velocities and positions based on the kinematics equations.

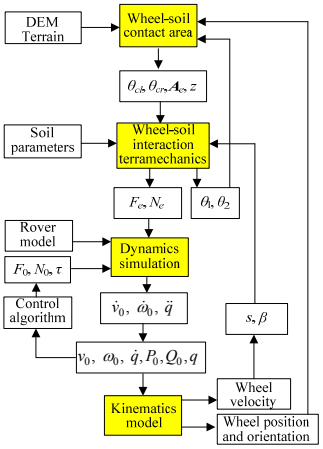

Fig. 5 Principle diagram of dynamics simulation

B. Experimental Validation

El-Dorado II, a four-wheeled mobile robot developed at SRL was used for validating the simulation. The robot has four F/T sensors to measure the wheel-soil interaction terramechanics. A visual odometry system was developed based on a telecentric camera to measure the position of the rover body and the slip ratio of wheels. The wheel entrance angles were measured with an angle meter for calculating the wheel sinkage. Two groups of experiments were performed. In group 1, the rover was applied resistance forces with counterweights from 0N to 60N, with a step of 10N, to generate different slip ratios. In group 2, the rover was controlled to climb up slopes from 0 to 15 degrees, with a step of 3 degrees, as shown in Fig. 6.

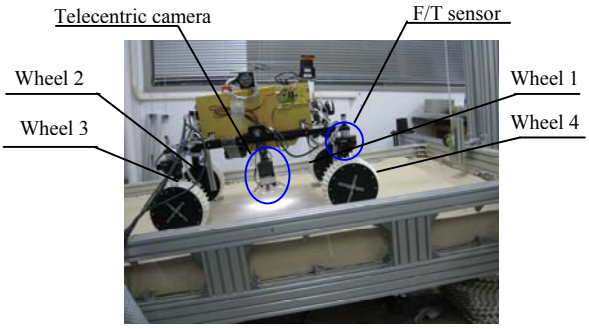

Fig. 6 Slope-climbing experiment with El-Dorado II robot

Parameters of the soft sand, which is called Toyoura, are identified with the experimental data: K_s=1796Kpa/m^N, c=24.5Pa, φ=35.75°, K=10.45mm. k_y is 19mm according to [12]. When the robot climbs up slopes, the remained parameters are: n_0=0.66, n_1=0.72, c_{P1}=-0.379, c_{P2}=0.616, c_{P3}=-0.448, C_M=0.214; while for the robot moving on flat terrain: n_0=0.63, n_1=0.72, c_{P1}=-0.276, c_{P2}= 0.633, c_{P3}=-0.304, C_M=0.354.

The comparison of the simulation and experimental results are shown in Figs. 7 and 8. Not only can the motion of the robot be predicted with high-fidelity, which is indicated by

the slip ratio, but also the drawbar pull, moment of resistance, as well as the normal force and wheel sinkage.

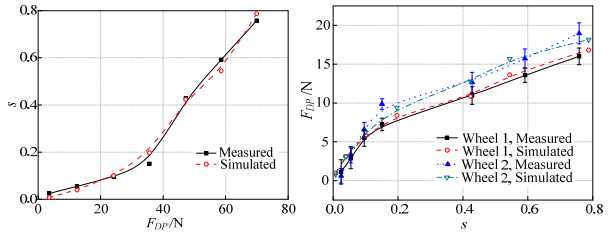

Fig. 7 Simulation and experimental results for robot moving on flat terrain

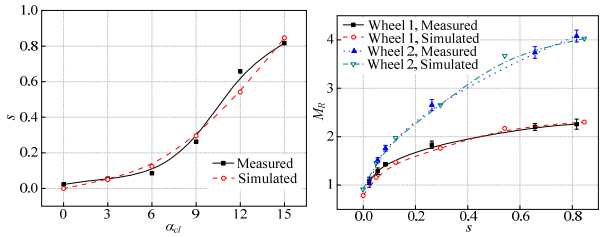

Fig. 8 Simulation and experimental results for robot climbing up slopes

C. *Simulation on Deformable Rough Terrain*

The robot was controlled to move from (0.5m, 0.5m) to (5m, 5m) on the random generated rough terrain shown in Fig. 9, with an initial yaw angle of 45 degrees. While moving, the robot deviates from the scheduled path because of the inclination angle of the terrain. Fig. 10 shows the slope angles that wheel 4 traversed over, RPY angles of the body and q_1, q_2 joint angles (q_1=-q_2), the slip ratios and normal forces.

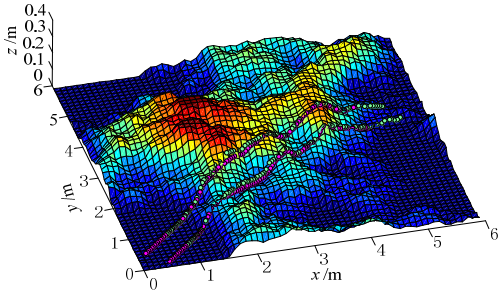

Fig. 9 Rough terrain and trajectories of wheels

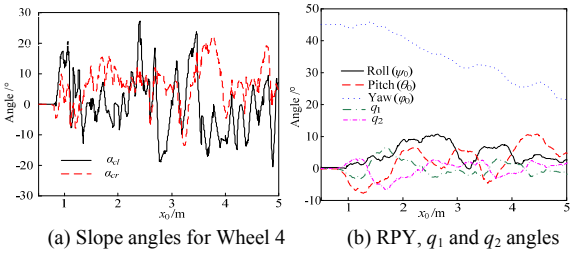

(a) Slope angles for Wheel 4 (b) RPY, q_1 and q_2 angles

(c) Slip ratios (d) Normal forces

Fig. 10 Simulation results for El-Dorado II moving on deformable rough terrain

VI. Conclusion and Future Work

The models of dynamics, wheel-soil interaction terramechanics and terrain presented in this paper is effective in simulate motion of robot moving on deformable rough terrain with a reasonable precision, verified by the experiments.

Future work should include the development of the skid model and steering model, validation of simulation results on rough terrain, and application of it for robot, such as design parameter optimization and control algorithm verification.

References

[1] L. Ding, H. Gao, Z. Deng, et al, "Design of comprehensive high-fidelity/high-speed virtual simulation system for lunar rover," in *Proc. 2008 IEEE Int. Conf. on Robotics, Automation and Mechatronics*, Chengdu, China, 2008: 1118-1123.

[2] J. Yen, A. Jain, and J. (Bob) Balaram, "ROAMS: rover analysis modeling and simulation software," in *Proc. 5th i-SAIRAS,* Noordwijk, Netherlands, 1999.

[3] A. Jain, J. (Bob) Balaram, J. Cameron, et al, "Recent developments in the ROAMS planetary rover simulation environment," in *Proc. IEEE Aerospace Conference Proceedings*, 2004: 861-875.

[4] G. SohL, and A. Jain, "Wheel-terrain contact modeling in the ROAMS planetary rover simulation," in *Proc. IDETC'05 ASME Int. Design Engineering Technical Conf. and Computers and Information in Engineering Conf*., Long Beach, CA, 2005.

[5] D. S. Apostolopoulos, "Analytical configuration of wheeled robotics locomotion," *The Robotics Institute of Carnegie Mellon University Technical Report CMU-RI-TR-01-08*, 2001.

[6] S. Michaud, L. Richter, N. Patel, et al, "RCET: rover chassis evaluation tools," in *Proc. 8th ESA Workshop on ASTRA*, ESTEC, Noordwijk, Netherlands, 2004.

[7] N. Patel, A. Ellery, E. Allouis, et al, "Rover mobility performance evaluation tool (RMPET): a systematic tool for rover chassis evaluation via application of bekker theory," in *Proc. 8th ESA Workshop on Advanced Space Technologies for Robotics and Automation*, ESTEC, Noordwijk, The Netherlands, 2004: 251-258.

[8] R. Bauer, W. Leung and T. Barfoot, "Development of a dynamic simulation tool for the Exomars rover," in *Proc. 8th i-SAIRAS*, Munich, Germany, 2005.

[9] http://www.astro.mech.tohoku.ac.jp/~ishigami/rover/.

[10] K. Yoshida, T. Watanabe, et al, "Terramechanics-based analysis and traction control of a lunar/planetary rover," in *Proc. 4th Int. Conf. on Field and Service Robotics*, Lake Yamanaka, Japan, 2003: 225-234.

[11] K. Yoshida and G. Ishigami, "Steering characteristics of a rigid wheel for exploration on loose soil," in *Proc. 2004 IEEE Int. Conf. on Intelligent Robots and Systems*, Sendai, Japan, 2004: 3995-4000.

[12] G. ISHIGAMI, "Terramechanics-based analysis and control for lunar/planetary exploration robots," Ph.D. dissertation, Tohoku University, Sendai, 2008.

[13] G. Ishigami, K. Nagatani and K. Yoshida, "Path planning for planetary exploration rovers and its evaluation based on wheel slip dynamics," in *Proc. IEEE ICRA.*, Roma, Italy, 2007: 2361-2366.

[14] L. Ding, H. Gao, Z. Deng, K. Yoshida and K. Nagatani, "Wheel-soil interaction mechanics model for planetary rover on loose soil considering lug effect and slip-sinkage," *Journal of ASME Applied Mechanics*, to be submitted for publication.

[15] Kazuya Yoshida, "The SpaceDyn: a MATLAB Toolbox for Space and Mobile Robots," *Journal of Robotics and Mechatronics*, 12 (4): 411-416.

[16] L. Ding, H. Gao, Z. Deng, K. Yoshida and K. Nagatani, "Slip ratio for lugged wheel of planetary rover in deformable soil: definition and estimation," in *Proc. 2009 IEEE/RSJ Int. Conf. Intelligent Robots and Systems*, St. Louis, MO, submitted for publication.

[17] L. Ding, H. Gao, Z. Deng, K. Yoshida and K. Nagatani, "Slip ratio for lugged wheel of planetary rover in deformable soil: definition and estimation," in *Proc. IEEE/RSJ Int. Conf. Intelligent Robots and Systems*, St. Louis, MO, 2009.